Relationship between growth speed, microstructure, mechanical and electrical properties in Bi-2212/Ag textured composites

Berdan ÖZKURT[a,*], M. A. Madre[b], A. Sotelo[b], M. Eyyüphan Yakıncı[c], Bekir Özçelik[d]

[a] Department of Electronic and Computer Education, Faculty of Tarsus Technical Education, University of Mersin, Mersin/Turkey

[b] ICMA (CSIC-Universidad de Zaragoza). María de Luna, 3. 50018 Zaragoza. Spain.

[c] Department of Physics, Faculty of Sciences and Letters, ˙Inönü University, 44069 Malatya, Turkey

[d] Department of Physics, Faculty of Sciences and Letters, Çukurova University, 01330 Adana, Turkey

Abstract

Transport properties on Bi-2212 superconductors can be improved by grain orientation methods while mechanical ones can be tuned up by the addition of metallic silver. Both processes can be performed simultaneously using the Laser Floating Zone (LFZ) method. In this work, $Bi_2Sr_2CaCu_2O_x$/3 wt.%Ag textured composite materials were prepared by a LFZ melting technique at different growth speeds (5, 15, 30, and 60 mm/h). In all cases, the observed microstructure after annealing shows the Bi-2212 phase as the major one. Although growth speed has no effect on the measured T_c values, a drastic

change on the J_c values has been found. The best results, both mechanical and transport properties, have been obtained for samples grown at 15 mm/h.

Keywords:

* Corresponding author. Tel.: +90 324 627 4804; fax: +90 324 627 4805

E-mail address: berdanozkurt@mersin.edu.tr

1. INTRODUCTION

The fabrication of bulk high-temperature superconductor with high electrical transport capacity at 77 K is of great interest for their practical applications [1]. In particular, BSCCO materials have demonstrated that they are suitable for many transport applications when they are properly processed in order to obtain a good grain orientation [2,3]. Among many techniques used successfully to produce well textured materials [4-6], the directional growth from the melt by the Laser Floating Zone (LFZ) method has demonstrated to be a very useful technique for producing well textured BSCCO rods at high growth rates [7-9]. As it was reported in previous works performed on laser textured materials [10], the microstructure of the superconducting ceramics is characterized by a good grain alignment, with their *c*-axis quasi-perpendicular to the growth direction. This high degree of texture leads to a very important increase of the transport properties, J_c, due to the reduction of the number of low-angle junctions [11]. On the other hand, due to the incongruent melting of this phase, after the growth process, it is necessary to perform an annealing in order to recombine the secondary phases to obtain the Bi-2212 one [12].

However, the poor mechanical properties of superconducting materials, due to their ceramic nature, impose limitations to their practical applications. Some attempts to improve their mechanical behaviour have been performed by high (~22wt.%) Ag additions on BSCCO sintered materials [13]. Further studies on textured materials have shown that the optimum Ag amount necessary to improve mechanical properties is much lower (1-3 wt.%) than for sintered materials [12] due to their lower porosity.

On the other hand, considering industrial production, it is necessary to acquire an improved understanding of the parameters related with the laser processing of such materials, avoiding the effect produced by the use of different precursors, as reported previously [14].

The aim of this work is determining the best growth conditions that yield optimum quality $Bi_2Sr_2CaCu_2O_x$/3wt.%Ag textured materials, using the LFZ technique. It is presented a comparison of directionally grown materials at different speeds from commercial $Bi_2Sr_2CaCu_2O_x$/3wt.%Ag composite powders.

2. EXPERIMENTAL

Green cylindrical precursors, 120 mm long and 3 mm diameter, approximately, have been prepared from commercial $Bi_{2.02}Sr_{2.02}Ca_{0.98}Cu_{1.99}O_x$/2.9wt.%Ag composite precursors (Nexans SuperConductors GmbH) by cold isostatic pressing with an applied pressure of 200 MPa during 1 minute. The obtained cylinders were used as feed in a directional solidification process which has been performed in a laser floating zone melting (LFZ) installation described elsewhere [15]. The bars have been processed using a continuous power Nd:YAG laser (λ=1064 nm), under air, at growth rates of 5, 15, 30, and 60 mm/h and a relative rotation of 18 rpm between seed and feed. The textured bars, about 150 mm length and 2 mm diameter, have shown to be very homogeneous dimensionally. After the texturing process, the resulting rods were cut into several pieces of ~30 mm long for the electrical characterizations and ~15 mm for the mechanical measurements.

As reported previously [14], the as-grown bars are composed of different secondary phases and it is necessary to perform a thermal treatment to

produce the Bi-2212 phase. This thermal treatment is composed of two different steps, the first one at 860 ºC during 60 h to form the Bi-2212 phase, followed by 12 h at 800 ºC to adjust the oxygen content, with a final quench to room temperature. Before the thermal treatment, four silver contacts were painted on the bars for the electrical measurements, two of about 5 mm at both ends of the bars for the current contacts and two small ones in the center of the bar for the voltage measurements. After the thermal treatments, the resulting silver contacts have typical resistances below 1 μΩ.

Phase determination has been performed on annealed samples using X-ray powder diffraction measurements (Rigaku D/max-B) with 2θ ranging between 10 and 60º. Microstructural characterization was made on polished longitudinal cross-sections of the samples, before and after the annealing process, in a scanning electron microscope (SEM, JEOL JSM 6400) equipped with an energy dispersive spectroscopy (EDX) system. After annealing, the proportion of the different phases has been estimated from several SEM micrographs using Digital Micrograph software.

Electrical measurements were performed by the conventional four-point probe configuration on about 30 mm long samples. Resistivity as a function of temperature, from 77 to 300 K, was measured using a dc current of 1 mA, in order to determine the transport T_c values. Critical current density (J_c) values were determined at 77 K, from the I-V curves, using the 1 μV/cm standard criterion.

Mechanical characterization has been performed by flexural strength, using the three-point bending test in an Instron 5565 machine with a 10 mm loading span fixture and a punch displacement speed of 30 μm/min.

3. RESULTS AND DISCUSSION

Fig. 1 shows SEM images corresponding to longitudinal polished sections of samples grown at different rates before annealing. In these images, five different phases can be found (marked in Fig. 1a for clarity), changing their proportion and orientation depending on the growth rate. The phase marked as #1 (dark grey contrast) corresponds to the Bi-free primary solidification phase, with composition (Sr,Ca)CuO_2. This phase appears well aligned with the rod axis, as expected from the flat solidification interface observed in the growth process [15], with an increased misalignment when the growth speed is increased. Light grey phase (marked as #2) shows a composition close to the ideal Bi-2201 stoichiometry. This phase's formation is promoted by its fast solidification kinetics from the Bi-enriched liquid, a process which follows initial nucleation of $(Ca_{1-x}Sr_x)CuO_2$. Moreover, from the trends observed in Fig. 1 it can be deduced that the grain growth of this Bi-rich phase mainly follows the alignment of the primary solidified phase. Grey phase, appearing only in the low growth speed samples, corresponds to the Bi-2212 phase (indicated by #3). Small black spots (marked as #4) distributed inside the Bi-rich phase have been identified as CaO particles. Finally, #5 is associated with Ag particles, which can be also seen as grey contrasts but can be distinguished by their shapes, as they tend to be spherical ones at high growth speeds while at lower ones they are aligned with the ceramic grains, filling the holes between them.

Other interesting features can be deduced from this figure, as the decrease on the grain alignment when the growth speed is increased from 5 to 60 mm/h. Moreover, it can also be clearly seen the increase of secondary phases proportion with the growth speed.

Powder XRD patterns, performed on textured and annealed samples, are displayed in Fig. 2. From this graphic, it is clear that the major peaks correspond to the Bi-2212 phase [16]. On the other hand, Ag is identified by the peak at around 39 º corresponding to the (111) plane [17]. These results confirm that the performed thermal treatment has been adequate for the Bi-2212 phase formation, independently of the growth speed. This is a very important point when taking into account that the quaternary Bi_2O_3-SrO-CaO-CuO system shows more than 20 stable phases [18]. Moreover, Ag addition modifies the phase relations of the Bi_2O_3-SrO-CaO-CuO system [19] making more difficult the determination of the optimal conditions for the Bi-2212 phase formation.

The microstructure of the annealed samples is presented in Fig. 3 where representative longitudinal polished sections for each growth speed are shown. The different contrasts found in these micrographs have been associated to different phases by EDX. Their composition, as well as their volume % (estimated using image analysis software) in the different samples, are displayed in Table I. From these micrographs and the data shown in Table I, it is evident that samples grown at 5 mm/h are nearly composed by the Bi-2212 phase accompanied by silver particles in a configuration which can be associated to the formation of a Bi-2212/Ag eutectic, in agreement with previously published works [19]. When growth speed is increased, besides the increase of secondary phases amount, the eutectic structure is destroyed and the $(Sr,Ca)_2CuO_3$ phase dissapears while two new phases are formed: $(Sr,Ca)CuO_2$ and CaO. On the other hand, the annealing process has also

produced a change on the Ag shape which is now elongated in all cases, filling the holes between superconducting grains.

Careful microstructural observations have led to the discovery of many intergranular cracks, indicated by arrows in Fig. 4, which are produced, during the annealing process, in the 5 mm/h grown samples. The cracks formation is probably due to the very big grain sizes obtained in these samples while they are not present in higher speed grown samples.

Flexural strength tests were made on annealed samples, grown at the different rates used in this work, in order to determine their mechanical behaviour. At least four samples for each growth speed were used to get more representative values. The mean maximum mechanical stress, together with its relative error, is represented in Fig. 5 for the different samples. At first sight, it is clear that lower growth speed increases mechanical strength due to the improved grain orientation. Samples grown at 5 mm/h do not follow the general evolution, but reduce their mechanical strength, compared with the 15 mm/h grown samples. This is a consequence of the cracks appearing in the 5 mm/h sample (see Fig. 4) which reduce significatively their mechanical properties. Moreover, the results dispersion is also higher for the 5 mm/h samples than fror the higher growth speeds due to the same crack effect.

Fig. 6 shows the temperature dependence of the resistivity as a function of growth speed. In this figure it can be clearly seen that T_c is approximately the same for all the samples. On the other hand, resistivity al room temperature increases with the growth speed until it reaches the maximum value for samples grown at 30 and 60 mm/h. This raise is due to the decrease of the grain alignment degree and the smaller grain sizes which increase the number of

grain boundaries along the samples. Moreover, it is also clear that the cracks observed in the 5 mm/h samples (see Fig. 4) are not affecting the transport properties for the small intensity currents (1 mA) used in the resistivity measurements. This result indicates that a continuous path for the electrical transport exists inside these samples in spite of the intergranular cracks found in the microstructure.

Fig. 7 shows the critical current density, at 77 K, *vs*. the growth speed. From this figure, it can be deduced that J_c increases when the growth speed is reduced, due to the better grain alignment and the higher grain sizes. On the other hand, it is also clear that samples grown at 5 mm/h deviate from this general trend due to the presence of cracks (see Fig. 4) in the samples which reduce the effective path for the current transport. As a consequence, the best results are obtained for samples grown at 15 mm/h with values around 3500 A/cm^2 which are about 20 % higher than the obtained for samples grown at 5 or 30 mm/h.

4. CONCLUSIONS

Composite $Bi_2Sr_2CaCu_2O_x$/3 wt.%Ag ceramics were successfully grown at different growth speeds from the melt, through a LFZ process. The amount and sizes of secondary phases is reduced when the growth speed is decreased leading to higher mechanical and electrical properties, except for samples grown at very low speeds due to the formation of intergranular cracks. It has been found an eutectic-like Bi-2212/Ag structure in samples grown at 5 mm/h. Best electrical and mechanical properties have been found for samples grown at 15 mm/h, with critical current density values of 3500 A/cm^2 (around 20 %

higher than the obtained for samples grown at 5 or 30 mm/h) and flexural strength of 180 MPa (around 13 and 29 % higher than the obtained for samples grown at 5 and 30 mm/h, respectively).

Acknowledgements

Berdan ÖZKURT acknowledges financial support from the TUBITAK for international mobility. M. A. Madre and A. Sotelo acknowledge financial support from the Spanish MICINN-FEDER (Projects MAT2008-00429 and MAT2008-05983) and the Gobierno de Aragón (Consolidated Research Group T12). The technical contributions of C. Estepa and C. Gallego are also acknowledged.

References

[1] M. Chen, L. Donzel, M. Lakner, W. Paul. J. Eur. Ceram. Soc. 24, 1815 (2004)

[2] F. P. Hermann. Handbook of Applied Superconductivity. IOP Publishing, Bristol (1998)

[3] M. Noe, K. P. Juengst, F. N. Werfel, S. Elschner, J. Bock, F. Breuer, R. Kreutz. IEEE Trans. Appl. Supercond. 13, 1976 (2003)

[4] V. Garnier, R. Caillard, A. Sotelo, G. Desgardin. Physica C 319, 197 (1999)

[5] M. S. Martin-Gonzalez, J. Garcia-Jaca, E. Moran, M. A. Alario-Franco. J. Mater. Res. 14, 3497 (1999)

[6] H. Maeda, K. Ohya, M. Sato, W. P. Chen, K Watanabe, M. Motokawa, A. Matsumoto, H. Kumakura, J. Schwartz. Physica C 382, 33 (2002)

[7] R. S. Feigelson, D. Gazit, D. K. Fork, T. H. Geballe. Science 240, 1642 (1988)

[8] A. Sotelo, M. A. Madre, J. C. Diez, Sh. Rasekh, L. A. Angurel, E. Martınez. Supercond. Sci. Technol. 22, 034012 (2009)

[9] M. Mora, A. Sotelo, H. Amaveda, M. A. Madre, J. C. Diez, F. Capel, J. M. López-Cepero. J. Eur. Ceram. Soc. 27, 3959 (2007)

[10] G. F. de la Fuente, M. T. Ruiz, A. Sotelo, A. Larrea, R. Navarro. Mater. Sci. Eng. A 173, 201 (1993)

[11] D. Shi. High Temperature Superconducting Materials Science and Engineering. Pergamon Press, Oxford (1995)

[12] A. Sotelo, M. Mora, M. A. Madre, J. C. Diez, L. A. Angurel, G. F. de la Fuente. J. Eur. Ceram. Soc. 25, 2947 (2005)

[13] A. Salazar, J. Y. Pastor, J. Llorca. Physica C 385, 404 (2003)

[14] A. Sotelo, Sh. Rasekh, M. A. Madre, J. C. Diez. J. Supercond. Nov. Magn. 24, 19 (2011)

[15] G. F. de la Fuente, J. C. Diez, L. A. Angurel, J. I. Peña, A. Sotelo, R. Navarro. Adv. Mater. 7, 853 (1995)

[16] T. A. Vanderah. Chemistry of superconductor materials. Noyes publications. New Jersey (1992)

[17] L. Lingun, W. A. Bassett. J. Appl. Phys. 44, 1475 (1973)

[18] P. Majewski. Supercond. Sci. Technol. 10, 453 (1997)

[19] P. Majewski, A. Sotelo, H. Szillat, S. Kaesche, F. Aldinger. Physica C 275, 47 (1997)

Table I. Phases composition determined by EDX, as well as their volume %, for the different samples.

Growth speed (mm/h)	Contrast	Composition	Vol. %
5	Dark grey	$(Sr,Ca)_2CuO_3$	1.0
	Grey	Bi-2212	92.0
	Light grey	Ag	3.0
	White	Bi-2201	4.0
15	Black	CaO	0.2
	Dark grey	$(Sr,Ca)CuO_2$	2.0
	Grey	Bi-2212	88.9
	Light grey	Ag	3.2
	White	Bi-2201	5.7
30	Black	CaO	1.0
	Dark grey	$(Sr,Ca)CuO_2$	3.5
	Grey	Bi-2212	85.8
	Light grey	Ag	2.7
	White	Bi-2201	7.0
60	Black	CaO	3.0
	Dark grey	$(Sr,Ca)CuO_2$	6.0
	Grey	Bi-2212	79.1
	Light grey	Ag	2.9
	White	Bi-2201	9.0

Figure captions

Figure 1. SEM micrographs of polished longitudinal sections of the Bi-2212/3 wt.%Ag textured materials before annealing: (a) 5; (b) 15; (c) 30; and (d) 60mm/h. The numbers indicate the different phases: 1) $(Sr,Ca)CuO_2$; 2) Bi-2201; 3) Bi-2212; 4); CaO; and 5) Ag.

Figure 2. Powder XRD patterns of the Bi-2212/3 wt.%Ag textured ceramic composites at different growth speeds (a) 5; (b) 15; (c) 30; and (d) 60mm/h. Bi-2212 diffraction peaks are identified by the corresponding crystallographic planes. Ag (111) peak is indicated by a #.

Figure 3. SEM micrographs of polished longitudinal sections of the Bi-2212/3 wt.%Ag textured materials after annealing: (a) 5; (b) 15; (c) 30; and (d) 60mm/h.

Figure 4. SEM micrograph of a polished longitudinal section of the Bi-2212/3 wt.%Ag grown at 5 mm/h showing the presence of intergranular cracks (indicated by arrows).

Figure 5. Annealed Bi-2212/3 wt.%Ag textured composites mechanical performance (three point flexure strength), together with their standard error, as a function of growth speed.

Figure 6. Temperature dependence of electrical resistivity on the annealed Bi-2212/3 wt.%Ag textured materials for the samples grown at different rates: ▲ 5, ▼ 15, ■ 30, and ● 60 mm/h.

Figure 7. Critical current density, at 77 K, *vs*. growth speed for the annealed Bi-2212/3 wt.%Ag textured composites.

Figure 1

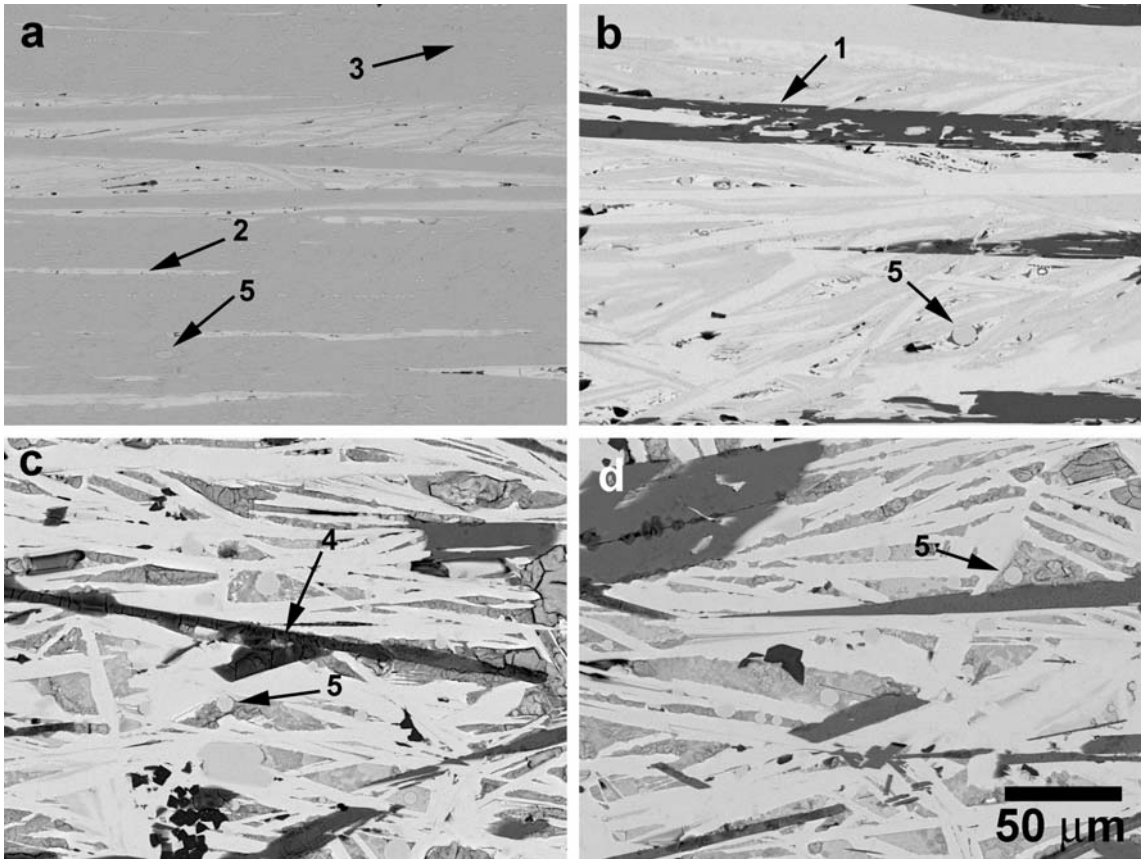

Figure 2

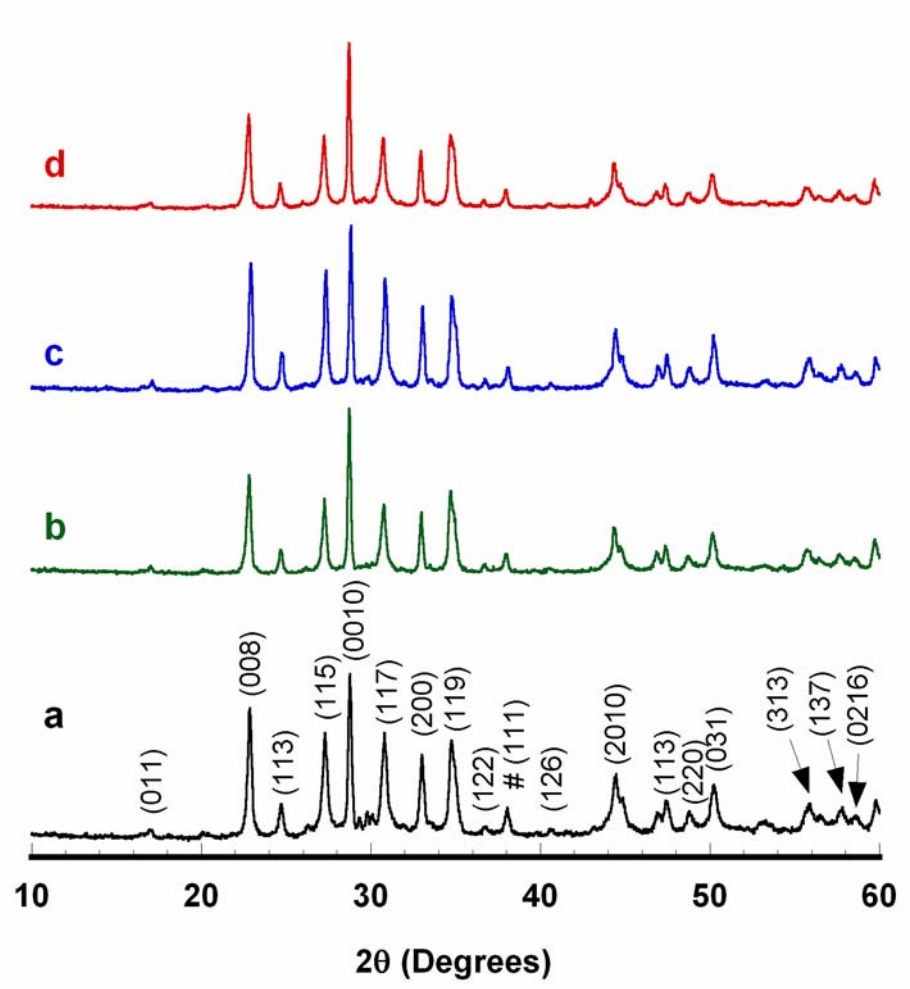
d
c
b
a
(011)
(008)
(113)
(115)
(0010)
(117)
(200)
(119)
(122)
(111)
(126)
(2010)
(113)
(220)
(031)
(313)
(137)
(0216)
10
20
30
40
50
60
2θ (Degrees)

Figure 3

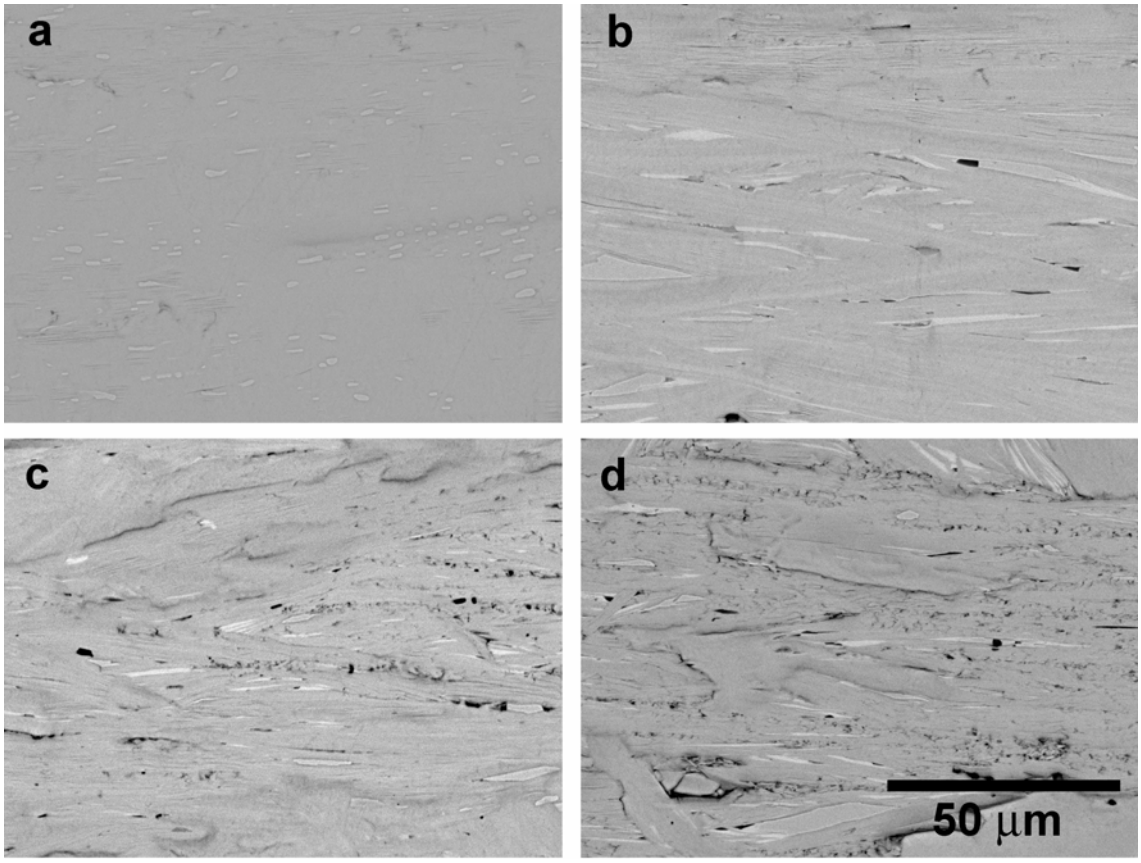

Figure 4

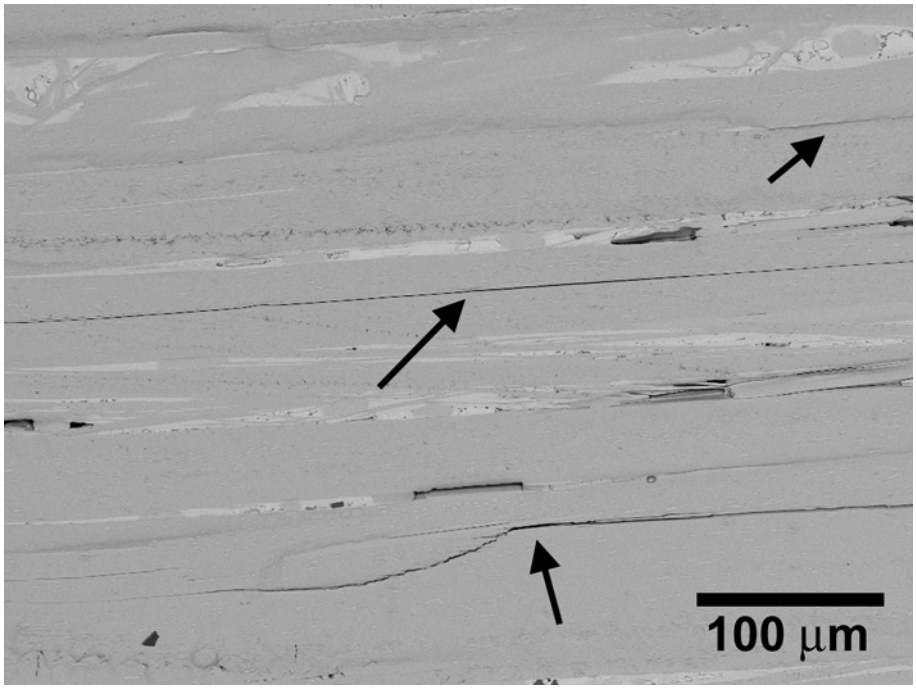

Figure 5

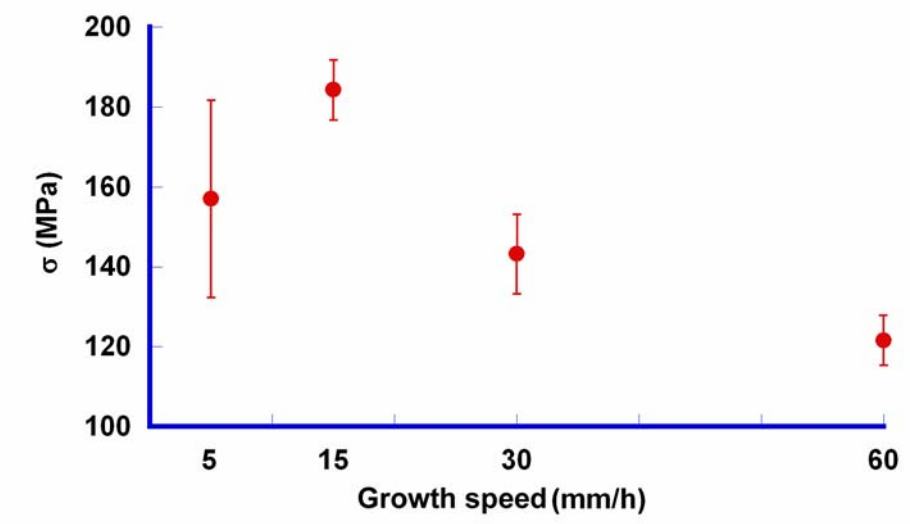

Figure 6

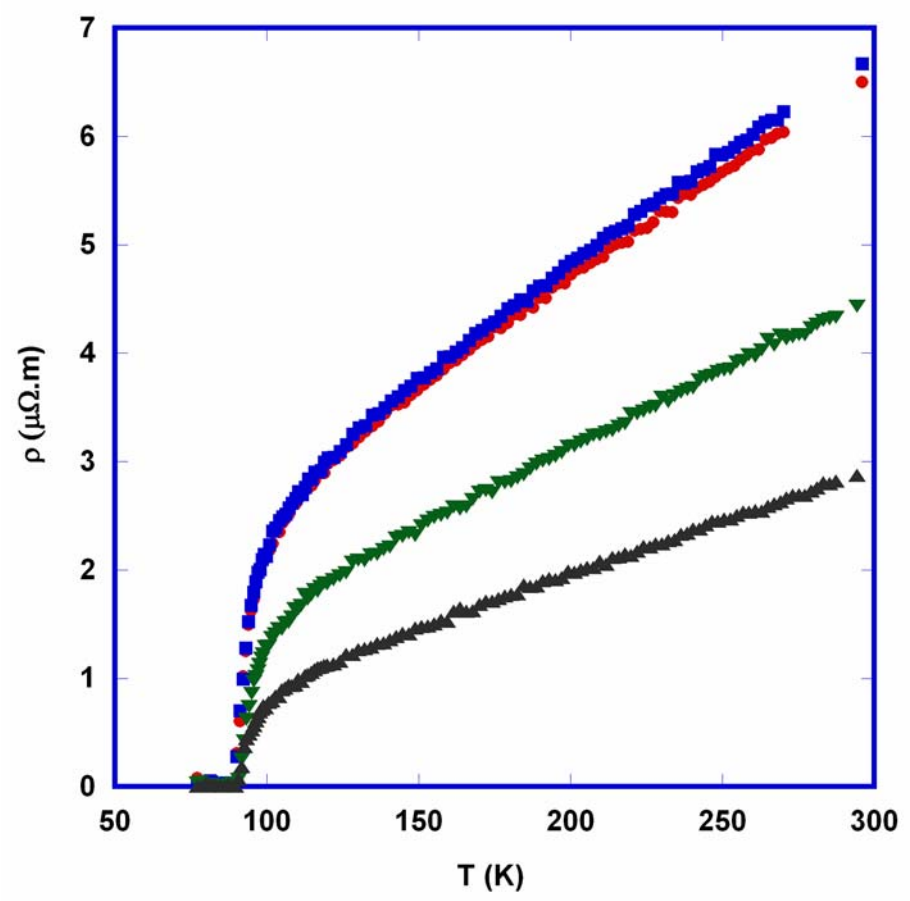

Figure 7

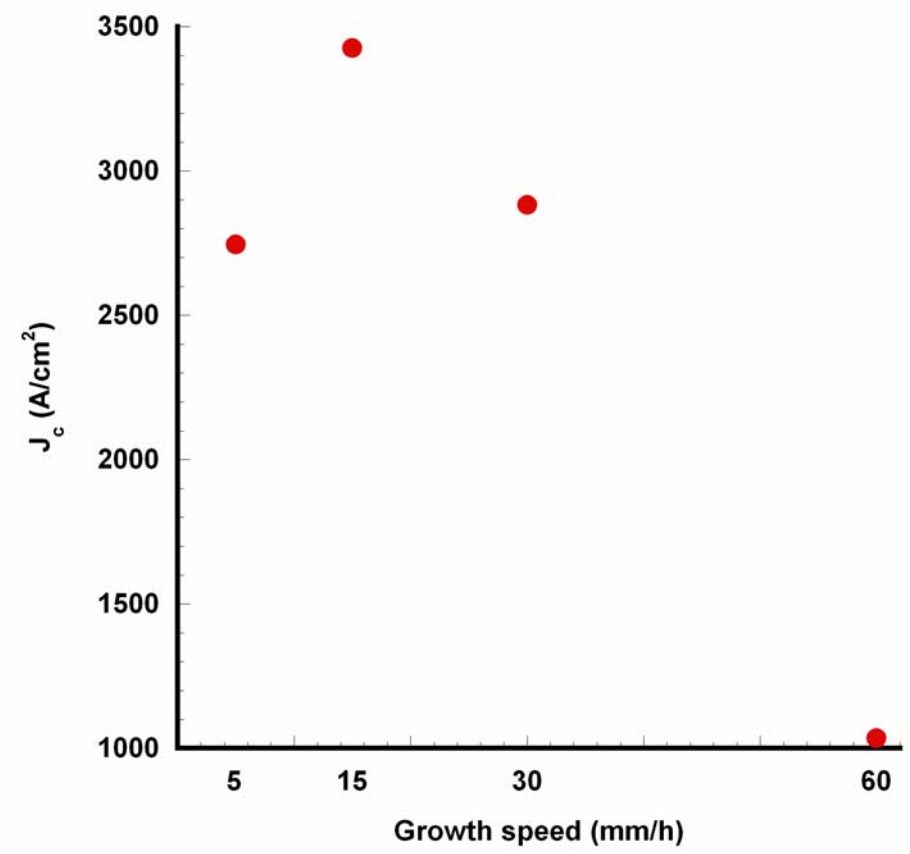
3500
3000
2500
2000
1500
1000
J_c (A/cm^2)
5
15
30
60
Growth speed (mm/h)